

(Sm,Zr)Fe_{12-x}M_x (M=Zr,Ti,Co) for permanent-magnet applications: *Ab initio* material design integrated with experimental characterization

Munehisa Matsumoto, Takafumi Hawaii, Kanta Ono
Institute of Materials Structure Science, High Energy Accelerator Research
Organization (KEK), Oho 1-1, Tsukuba, Ibaraki 305-0801, Japan
(Dated: May 19, 2020)

In rare-earth permanent magnets (REPM's), trade-off's between intrinsic magnetic properties are often encountered. A recent example is SmFe₁₂ where excellent magnetic properties can be achieved at the sacrifice of bulk structure stability. Bulk structure stability is sustained by the presence of the third substitute element as is the case with SmFe₁₁Ti, where Ti degrades magnetic properties. It is now in high demand to find out with which chemical composition a good compromise in the trade-off between structure stability and strong ferromagnetism is reached. We inspect the effects of representative substitute elements, Zr, Ti, and Co in SmFe₁₂ by combining *ab initio* data with experimental data from neutron diffraction. The trend in the intrinsic properties with respect to the concentration of substitute elements are monitored and a systematic way to search the best compromise is constructed. A certain minimum amount of Ti is identified with respect to the added amount of Co and Zr. It is found that Zr brings about a positive effect on magnetization, in line with recent experimental developments, and we argue that this can be understood as an effective doping of extra electrons.

PACS numbers: 75.50.Ww, 75.25.+z, 75.10.Lp, 61.12.Ld

I. INTRODUCTION

Rare-earth permanent magnet (REPM) based on Nd₂Fe₁₄B¹⁻⁴ have been in commercial use in the past several decades. Nd-Fe-B ternary alloys based on R₂Fe₁₄B (R=rare earth including Nd) make excellent permanent magnets except for a caveat on relatively low Curie temperature: the Curie temperature of Nd₂Fe₁₄B is 585 K, which is only marginally beyond the typical high-temperature edge at 450 K of practical use in traction motors and power generators. Thus a way to supplement the high-temperature properties has been pursued in various respects, most notably addition of heavy-rare-earth elements to help high-temperature coercivity via enhancing the high-temperature anisotropy field⁵. Along the line of searches for alternative materials with higher Curie temperature or/and improved temperature coefficient of magnetization and anisotropy field, NdFe₁₂N⁶⁻⁸ and Sm(Fe,Co)₁₂⁹ recently have triggered renewed interest in ferromagnets with the ThMn₁₂-type crystal structure as shown in Fig. 1. It has been shown both theoretically⁶ and experimentally^{7,9} that the intrinsic magnetism of 100% Fe-based ferromagnets with the ThMn₁₂ structure may potentially be superior to Nd₂Fe₁₄B if the bulk structure stability is guaranteed, which is so far achieved only on a special substrate in laboratory. Originally it was only a few years after the discovery of Nd₂Fe₁₄B that the material based on the ThMn₁₂ crystal structure had been found¹⁰, but the drawback that the particular ThMn₁₂ crystal structure is only metastable for RFe₁₂ (R=rare earth) had hindered further developments. The problem is not yet entirely eliminated even today^{11,12}, but persistent efforts to bring the structure stability closer^{13,14} and recent renewed efforts^{15,17-21} together with the advent of various ways of data exploitation may

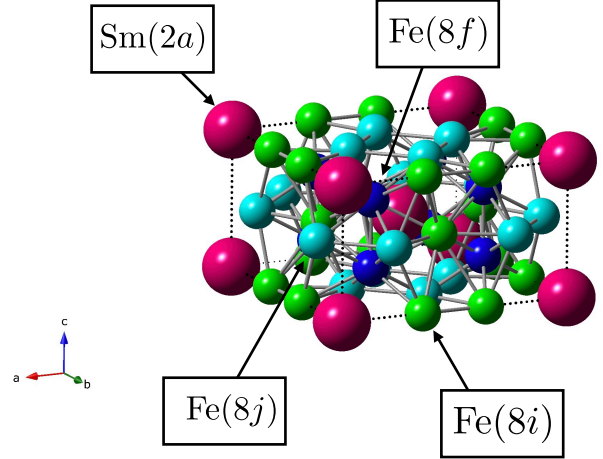


FIG. 1. (Color online) Crystal structure of SmFe₁₂. Large and red balls represent Sm(2a) sites and green/cyan/blue and small balls represent Fe(8i)/Fe(8j)/Fe(8f) sites, respectively. In the tetragonal box shown here, two formula units are included.

change the perspective. This work presents an attempt to combine theoretical and experimental data to work with the severe trade-off that is almost always encountered among the prerequisites for a ferromagnet to make a good main phase of REPM, namely, strong magnetization, accordingly strong uni-axial magnetic anisotropy, high Curie temperature, and good structure stability, for the particular case of SmFe₁₂.

This paper is organized as follows. In the next section we outline our methods that incorporate both of experimental data and theoretical data. For the theory part,

the details of *ab initio* calculations are given in Sec. A. Main results are shown in Sec. III: structure stability is inspected on the basis of calculated formation energy in Sec. III A, and one of the main messages therefrom for the site preference of the substitute element Zr is confirmed via data integration between experiment and theory in Sec. III B. Trends in the magnetic properties are inspected in Sec. III C and an optimal concentration in the middle of the trade-off between the structure stability and the magnetic properties is identified. In Sec. IV we discuss the results in the light of old and recent experimental findings. Conclusions and outlook are described in Sec. V. Details of calculations and data analyses are encapsulated in Appendix so that the presentation can be followed straightforwardly and also in a self-contained way.

II. METHODS AND TARGET MATERIALS

A. *Ab initio* inspection on the effects of substitute elements in SmFe_{12}

Effects of substitute elements, Zr, Ti, and Co on pristine SmFe_{12} are investigated by calculating the formation energy and intrinsic magnetic properties from first principles. Formation energy is obtained through *ab initio* structure optimization based on generalized gradient approximation (GGA)²², which is known to predict reasonable lattice parameters for most of the Fe-based ferromagnets. Lattice parameters out of the structure optimization for SmFe_{12} is summarized in Table I together with counterpart numbers from previous theoretical²³ and experimental⁹ works. Calculated energy of SmFe_{12} is subtracted by with the summation of calculated total energy of the ingredient elements and we inspect how much formation energy is gained by the substitute elements. Details of these *ab initio* calculations are given in Appendix A.

As has been shown in Fig. 1, the crystal structure of SmFe_{12} is characterized by multiple sublattices, namely, $\text{Sm}(2a)$, $\text{Fe}(8i)$, $\text{Fe}(8j)$, and $\text{Fe}(8f)$. *Ab initio* studies showed the relative trends in magnetic moment $m[r]$ on site r as $m[\text{Fe}(8i)] > m[\text{Fe}(8j)] > m[\text{Fe}(8f)]$ in RFe_{12} ⁶. A guiding principle for the possible design of an optimal material would be to keep the magnetization from $\text{Fe}(8i)$ as much as possible while gaining structure stability, but unfortunately the preference of the substitute Ti atom goes for the $\text{Fe}(8i)$ site from $T = 0$ all the way to higher temperatures²⁴, which we also confirm for $T = 0$ as shown in Fig. 2. Thus the dominant magnetic moment from $\text{Fe}(8i)$ is sacrificed while achieving the bulk structure stability. Given this trade-off, control of the chemical composition toward a better compromise has been pursued in the following way^{13,14}: the structure stability can be gained by Zr partly replacing $\text{Sm}(2a)$ and thus the amount of Ti to stabilize the crystal structure might be able to be reduced, leading to an improved magneti-

	Pristine		Alloy	
	Calc.	Expt.	Calc.	Expt.
	this work	Ref. 23	Ref. 9	this work
				$\text{Zr}(2a) / \text{Zr}(8i)$
a (Å)	8.569	8.497	8.35	8.507
c (Å)	4.735	4.687	4.81	4.770
c/a	0.5525	0.5516	0.576	0.5607
x_i	0.3590	0.3588		0.3562 / 0.3553
x_j	0.2712	0.2696		0.2764 / 0.2768

TABLE I. Our *ab initio* lattice parameters from structure optimization for the pristine material SmFe_{12} , compared to a few previous works^{9,23}, and our lattice parameters for SmFe_{12} (Zr-substituted $\text{Sm}(\text{Fe},\text{Co},\text{Ti})_{12}$) derived from the self-consistent analysis between *ab initio* calculations and Rietveld analysis of neutron diffraction data. The internal coordinates x_i and x_j are defined in Appendix. A 1.

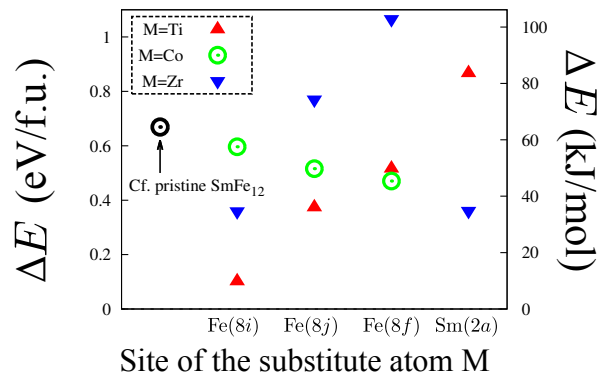


FIG. 2. (Color online) Calculated formation energy, ΔE , of SmFe_{12} with substitute elements Ti, Co, or Zr. In the tetragonal unit shown in Fig. 1 containing two formula units of SmFe_{12} , one substitute atom, either Ti, Co, or Zr, replaces one host atom and *ab initio* structure optimization is done to extract the formation energy per formula unit (f.u.).

zation. Now a question can arise concerning the nature of substitute Zr, which should be chemically similar to Ti, being on the same family on the periodic table of elements: how can the preference of host sublattice be so drastically different between Ti and Zr? Indeed our calculations of formation energy of Zr-substituted SmFe_{12} , exploring all possible sublattices for the substitute Zr atom, show that Zr energetically favors $\text{Fe}(8i)$ site as well as $\text{Sm}(2a)$ site as shown in Fig. 2. In contrast, recent investigations on $(\text{Sm},\text{Zr})(\text{Fe},\text{Co},\text{Ti})_{12}$ are in progress presuming that Zr atom mostly replaces $\text{Sm}(2a)$ ²⁰. Precise understanding on the roles of Zr, Co, and Ti in SmFe_{12} seems to be in acute need.

B. Integration between *ab initio* data and Rietveld analysis of neutron diffraction experiment

In order to take a closer look into the experimental facts for Zr-substituted SmFe_{12} , we combine *ab initio* inputs and outputs with our experimental data from neutron diffraction. Here the powder sample of $\text{Sm}_{0.8}\text{Zr}_{0.2}(\text{Fe}_{0.75}\text{Co}_{0.25})_{11.25}\text{Ti}_{0.75}$ was provided by Toyota Motor Corporation and the powder neutron diffraction measurements at room temperature were performed on ECHIDNA at Australian Nuclear Science and Technology Organisation (ANSTO)²⁵. Rietveld analysis of diffraction data²⁶ gives the lattice constants and the internal coordinates of Fe(8*i*) and Fe(8*j*) in the unit cell. These are plugged into *ab initio* calculations using coherent potential approximation (CPA)²⁷ based on local density approximation (LDA) following Vosko, Wilk, and Nusair²⁸ which is known to give reasonable magnetic moments on a given crystal structure. We make a few steps further: calculated magnetic moment on each atom is fed back into the Rietveld analysis of diffraction data to obtain the refined input data consisting of lattice constants and internal coordinates²⁹. We observe that this overall self-consistent iteration loop between Rietveld-analysis of experimental data *ab initio* calculations converges in quite a fast and robust way. We would tentatively refer to this particular combination of theory and experiment as “LDA+Rietveld”. Detailed data during the overall iteration procedure can be found in the Appendix B. Combination of the Rietveld analysis with *ab initio* calculation to verify the structure stability has been widely done recently^{31,32}, while the way to reinforce the convergence of the data via the feedback between theory and experiment is new to the best of the authors’ knowledge. Here the scope of the problem imposed on the Rietveld analysis is slightly different from the conventional one for the structure analysis: our lattice structure space is limited, restricting ourselves on the given prototype of ThMn_{12} structure, while the details of the sublattice-resolution in the multiple-sublattice ferromagnetism is the present problem. In such a restricted working space, the feedback between theory and experiment can be implemented directly and easily. The scheme for this type of self-consistent iteration is shown in Fig. 3 and the initial shot of the Rietveld analysis is shown in Fig. 4.

For the assessment of magnetic anisotropy in the typical working temperature range, one of the most influential factors is actually an indirect exchange coupling between rare earth atom and Fe atom³³. We use Sm(5*d*)-Fe(3*d*) exchange coupling as a key descriptor for the leading-order of the finite-temperature anisotropy field which intrinsically controls the finite-temperature coercivity. Thus we actually do without spin-orbit interaction in our *ab initio* calculations. Even though we do not directly address the uni-axial magnetic anisotropy, inspection of linear trends in the leading order contribution around a reasonable limit at the pristine SmFe_{12} would do. This simplifies the theory part and enable a

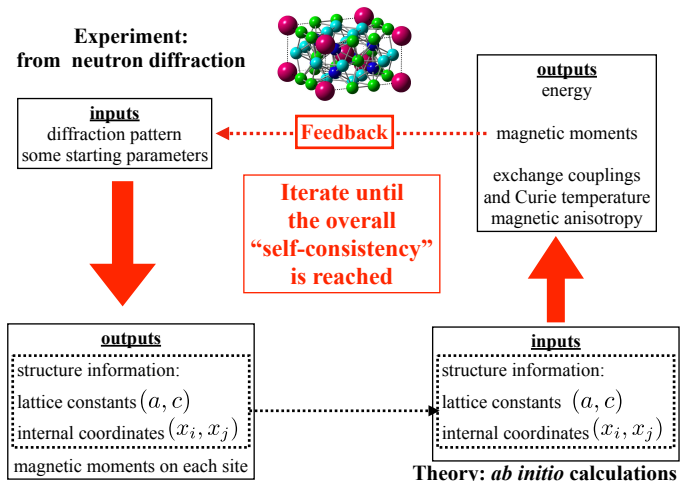


FIG. 3. (Color online) The scheme of the “LDA+Rietveld” self-consistent iterations.

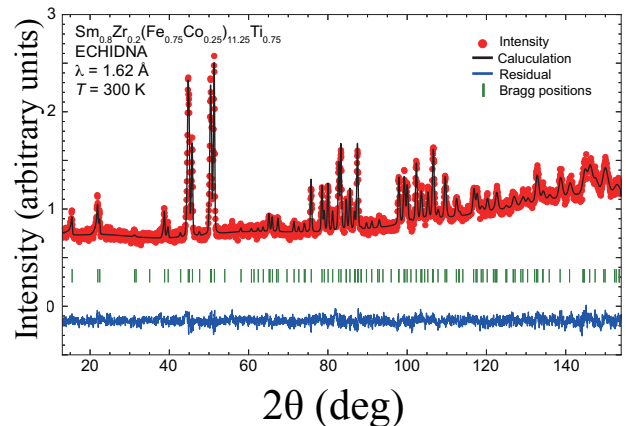


FIG. 4. (Color online) The initial shot of the Rietveld analysis of which output makes an initial input to *ab initio* KKR-CPA in the overall “LDA+Rietveld” iteration.

wide coverage of parameter space spanned by the chemical composition. Our target observables consist of the formation energy, magnetization, and inter-atomic exchange couplings out of which Fe-Fe couplings control the Curie temperature and Fe-Sm couplings control the room-temperature anisotropy field.

III. RESULTS

A. Calculated formation energy of SmFe_{12}

We inspect the influence of each substitute element, Ti, Co, and Zr, in SmFe_{12} on the structure stability based on the derivative of calculated formation energy

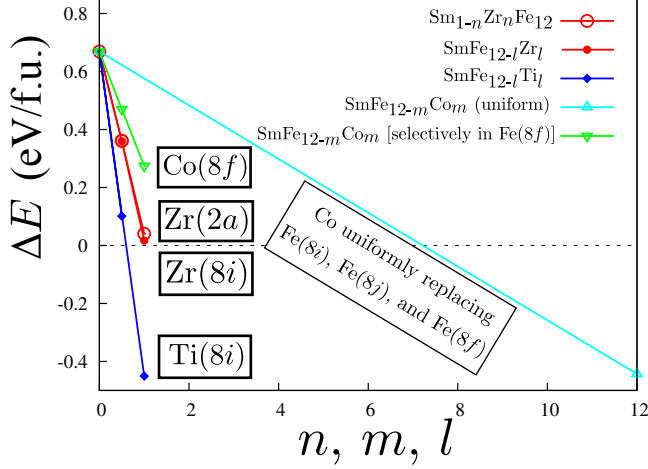


FIG. 5. (Color online) Calculated formation energy of SmFe_{12} per formula unit (f.u.) as a function of the concentration of substitute elements. In these calculations, the substitute elements are selectively put into the most energetically favorable sublattice, unless otherwise stated.

substitute	$U_{\Delta E} \equiv (-\partial\Delta E)/\partial n_M$ (eV/f.u.)
Zr in Sm(2a)	0.63
Zr in Fe(8i)	0.62
Ti in Fe(8i)	1.13
Co (uniformly substituting)	0.093
Co in Fe(8f)	0.4

TABLE II. Derivative of the formation energy of SmFe_{12} per formula unit (f.u.) around the pristine limit with respect the number of substitute elements per formula unit.

ΔE with respect to the concentration of substitute elements and see how the amount of Ti can be reduced with the possible help from Zr and Co to be on a par with $\text{SmFe}_{11}\text{Ti}$ concerning the structure stability. Negative and large absolute value of the formation energy is beneficial. The exact formula and values of calculated energy are summarized in Appendix A1. The results for SmFe_{12} have been shown in Fig. 2. Observing the minimum energy among the multiple choices for the substitute elements, the preference of substituting Ti goes for Fe(8i), Co does for Fe(8f), both in agreement with the claims of past works^{24,34}, while the conclusion for Zr from this data set may not be entirely consistent with recent experimental developments for SmFe_{12} : Zr in Fe(8i) and Zr in Sm(2a) look almost degenerate energetically in our data while Zr substituting mostly Sm(2a) is seen in the literature²⁰. Formation energy is summarized as a function of concentration as shown in Fig. 5. Utility of a substitute element M may be characterized by a differential coefficient, $(-\partial\Delta E/\partial n_M)$, where n_M is the number of substitute element M per formula unit.

From the data shown in Fig. 5 the coefficients are extracted as shown in Table. II. Ti indeed works for the structure stability most effectively. For our target compound $(\text{Sm}_{1-n}\text{Zr}_n)(\text{Fe}_{12-m-l-l'}\text{Co}_m\text{Ti}_l\text{Zr}_{l'})$, where n is the number of Zr atoms substituting Sm(2a), m is the number of substituting Co atoms per formula unit, l is the number of substituting Ti atoms in the Fe(8i) sublattice per formula unit, and l' is the number of substituting Zr atoms in the Fe(8i) sublattice per formula unit, to be better or on a par with $\text{SmFe}_{11}\text{Ti}$ concerning the formation energy, the following condition must be met:

$$nU_{\Delta E}(\text{Zr}(2a)) + mU_{\Delta E}(\text{Co}) + lU_{\Delta E}(\text{Ti}) + l'U_{\Delta E}(\text{Zr}(8i)) \gtrsim (1/12)U_{\Delta E}(\text{Ti}).$$

Assuming uniform substitution by Co considering the relatively minor preference of Co substituting in SmFe_{12} , the following relation is imposed.

$$0.63n + 0.093m + 1.13l + 0.62l' \gtrsim 1.13 \quad (1)$$

With our sample having 0.2 Zr atoms, thus the relation $n + l' = 0.2$ is imposed, and $\lesssim 25\%$ of Co atoms per formula unit, we end up with the following condition,

$$0.279 + 0.63n + 0.62(0.2 - n) \gtrsim 1.13(1 - l), \quad (2)$$

which gives us the lower bound on l as $0.643 - 0.009n$ ($0 \leq n \leq 0.2$): almost independently of how Zr atoms are distributed over Sm(2a) or Fe(8i) sublattices, the minimum amount of Ti can be reduced to the smaller number than $\text{SmFe}_{11}\text{Ti}$ by 35%. Thus we quantitatively confirm that Zr in Sm(2a), partly also in Fe(8i), and uniformly substituting Co indeed enables the reduction of Ti concerning the formation energy.

B. LDA+Rietveld results for Zr-substituted $\text{Sm}(\text{Fe}, \text{Co}, \text{Ti})_{12}$

Having confirmed the assumed utility of Zr for the structure stability from first principles, we inspect the real sample of $\text{Sm}_{0.8}\text{Zr}_{0.2}(\text{Fe}_{0.75}\text{Co}_{0.25})_{11.25}\text{Ti}_{0.75}$ to see how the calculated site preference may be reflected in experimental reality. Rietveld analysis is performed to extract the localized magnetic moments, concentration distribution of component elements occupying the same sublattice, internal coordinates, and lattice constants. Out of these outputs from the experimental data analysis, the lattice structure information typically make the inputs to *ab initio* calculations in order to do the simulations of the complicated multiple-sublattice material as realistically as possible. *Ab initio* structure optimization does illustrate the relative trends but it does not always pin-point the quantitative results from experimental measurements, as is seen in Table I. Detailed and reliable inputs for the internal coordinates as well as the

lattice constants, such as reported in Ref. 35 for YFe_{11}Ti , have been in great demand to address the subtle interplay among various contributions from different sublattices and the trade-off between prerequisite properties for multiple-sublattice magnets.

Given the structural inputs, *ab initio* calculations yield electronic structure including magnetic moment on each atom: these outputs can now be recycled as a renewed input to the Rietveld analysis so that the solution of the inverse problem to decode the neutron diffraction pattern would be more robust²⁹. We have iterated such feedback process from *ab initio* outputs to Rietveld analysis in the next step until self-consistency is reached, now following Korringa-Kohn-Rostoker (KKR) Green's function method combined with coherent potential approximation (CPA) for alloys²⁷. The details of the computational setup and the specific way the overall iteration proceeds are described in Appendix B. Remarkably, the convergence down to 5-6 digits is achieved within a few iteration steps, counting a set of Rietveld analysis and *ab initio* calculation as one step. Here the self-consistency is identified by reaching a fixed point of the iterative loop where the input and output information become identical within the numerical precision.

As long as the calculated energy within KKR-CPA is concerned, the energy of the electronic structure is not minimized as the consistency between theory and experiment is approached as seen in Table. V in Sec. B below. Systematic deviation between experiment and theory concerning the lattice constant is reasonable considering the fact the experiments are done at room temperature while *ab initio* calculations are for zero temperature³⁰. The difference of working temperatures between theory and experiment should not be a problem as long as the intrinsic Curie temperature is high enough to ren-

der the room-temperature properties close to the ground state. It is to be noted that the LDA+Rietveld analysis at this stage is not a variational framework with respect to the intrinsic energy of the electronic state but a generalized data fitting technique assisted by the guideline data provided from first principles.

We observe that either case of $\text{Sm}(2a)$ taking Zr or $\text{Fe}(8i)$ taking Zr is equally plausible, in line with the site preference inspected with the *ab initio* structure optimization. The resultant lattice constants have been summarized in Table I. The detailed quantitative distribution of Zr over $\text{Sm}(2a)$ and $\text{Fe}(8i)$ has not been entirely determined here due to a problem with Zr in the Rietveld analysis of the neutron diffraction data in that magnetic moment on Zr may be too small. At least we have seen that there should be some finite contribution from Zr atoms substituting the $\text{Fe}(8i)$ sublattice.

C. Optimal chemical composition with SmFe_{12}

Now the prerequisite magnetic properties for REPM are inspected. The observables are magnetization, Curie temperature as obtained on the basis of mean-field approximation for calculated exchange couplings between *d*-electrons, and the *5d-3d* exchange couplings that indirectly binds *4f* and *3d* electrons together as a key measure for finite-temperature magnetic anisotropy³³. The last observable is denoted as “ J_{RT} ”, emphasizing that this is the coupling between rare-earth atom (R) and transition-metal atom (T). For SmFe_{12} there are three sublattices for Fe and accordingly J_{RT} has three variants $J_{\text{RT}}(8i)$, $J_{\text{RT}}(8j)$, and $J_{\text{RT}}(8f)$. Calculated results of them for doped SmFe_{12} , here we denote as $\text{Sm}_{1-n}\text{Zr}_n(\text{Fe}_{12-m-l-l'}\text{Co}_m\text{Ti}_l\text{Zr}_{l'})$ for each of the focus elements: Ti, Co, and Zr, are shown in Appendix C.

The partial derivative coefficients of the target observables M , T_{Curie} , J_{RT} for $\text{Fe}(8i)$, $\text{Fe}(8j)$, and $\text{Fe}(8f)$, with respect to the number of the substitute elements around the pristine limit, n , m , l , and l' , per formula unit, SmFe_{12} ²³, can be summarized as follows. The detailed derivation of this working matrix is given in Table VI in Appendix.

$$\begin{aligned}
 & \begin{pmatrix} (\partial M/\partial n)/M & (\partial M/\partial m)/M & (\partial M/\partial l)/M & (\partial M/\partial l')/M \\ (\partial T_{\text{Curie}}/\partial n)/T_{\text{Curie}} & (\partial T_{\text{Curie}}/\partial m)/T_{\text{Curie}} & (\partial T_{\text{Curie}}/\partial l)/T_{\text{Curie}} & (\partial T_{\text{Curie}}/\partial l')/T_{\text{Curie}} \\ \{ \partial J_{\text{RT}}(8f)/\partial n \} / J_{\text{RT}}(8f) & \{ \partial J_{\text{RT}}(8f)/\partial m \} / J_{\text{RT}}(8f) & \{ \partial J_{\text{RT}}(8f)/\partial l \} / J_{\text{RT}}(8f) & \{ \partial J_{\text{RT}}(8f)/\partial l' \} / J_{\text{RT}}(8f) \\ \{ \partial J_{\text{RT}}(8i)/\partial n \} / J_{\text{RT}}(8i) & \{ \partial J_{\text{RT}}(8i)/\partial m \} / J_{\text{RT}}(8i) & \{ \partial J_{\text{RT}}(8i)/\partial l \} / J_{\text{RT}}(8i) & \{ \partial J_{\text{RT}}(8i)/\partial l' \} / J_{\text{RT}}(8i) \\ \{ \partial J_{\text{RT}}(8j)/\partial n \} / J_{\text{RT}}(8j) & \{ \partial J_{\text{RT}}(8j)/\partial m \} / J_{\text{RT}}(8j) & \{ \partial J_{\text{RT}}(8j)/\partial l \} / J_{\text{RT}}(8j) & \{ \partial J_{\text{RT}}(8j)/\partial l' \} / J_{\text{RT}}(8j) \end{pmatrix} \\
 &= \begin{pmatrix} 0.0244238 & 0.0302537 & -0.189388 & -0.177486 \\ 0.196759 & 0.234125 & -0.0047857 & -0.0697258 \\ 0.0955673 & 0.0831466 & -0.0480785 & -0.0926378 \\ 0.116806 & 0.0804769 & 0.0804248 & 0.0335155 \\ 0.135327 & 0.0614006 & -0.036302 & -0.0497742 \end{pmatrix} \quad (3)
 \end{aligned}$$

Each element in the above derivative matrix has been normalized by the absolute values at the pristine limit.

The derivative matrix in Eq. (3) shows that Zr atom

substituting the $\text{Sm}(2a)$ sublattice and Co atom substi-

tuting uniformly the overall Fe sublattice works almost on a par, positively for the intrinsic magnetic properties. The positive effect of Zr seems to be consistent with the recent experimental observation²¹ and the microscopic mechanism is discussed below in Sec. IV B.

On the other hand, Ti or Zr substituting the Fe(8i) sublattice is detrimental to almost all properties. The only positive effect of Ti(8i) and Zr(8i) is seen on the Fe(8i)-Sm(2a) exchange coupling, which is the nearest-neighbor exchange path between Sm and Fe.

With the quantified effects of substitute elements Ti, Co, and Zr in SmFe₁₂, we put forward a formulation of the trade-off problem described in Sec. I. The target material Sm_{1-n}Zr_nFe_{12-m-l-l'}Co_mTi_lZr_{l'} can be characterized by an overall target function $U_{\text{all}}(\{U_{\Delta E}, U_M, U_{T_c}, U_{J_{\text{RT}}(8f)}, U_{J_{\text{RT}}(8i)}, U_{J_{\text{RT}}(8j)}\})$ that is to be defined in terms of partial target function for each of the observables that can be defined referring to Eqs. (1) and (3):

$$U_{\Delta E} \equiv (0.63n + 0.093m + 1.13l + 0.62l' - 1.13)/(\Delta E_0)$$

$$U_M \equiv 0.0244n + 0.0303m - 0.189l - 0.177l'$$

$$U_{T_c} \equiv 0.197n + 0.234m - 0.00479l - 0.0697l'$$

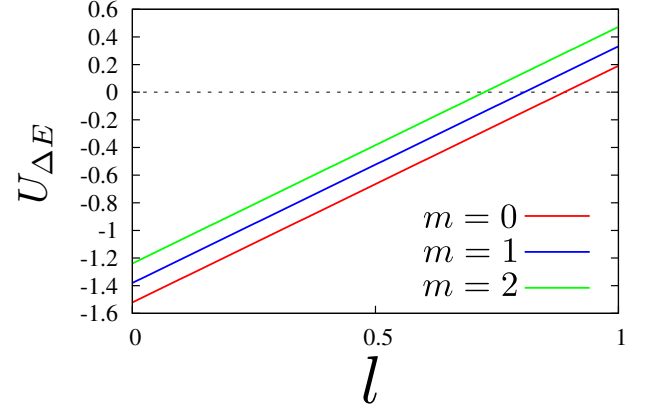
$$U_{J_{\text{RT}}(8f)} \equiv 0.0956n + 0.0831m - 0.0481l - 0.0926l'$$

$$U_{J_{\text{RT}}(8i)} \equiv 0.117n + 0.0805m + 0.0804l + 0.0335l'$$

$$U_{J_{\text{RT}}(8j)} \equiv 0.135n + 0.0614m - 0.0363l - 0.0498l'.$$

Here ΔE_0 is a reference formation energy which we take as the number at the pristine limit shown in Fig. 2. We note that the expansion around the pristine limit should be used only within the linear regime in the overall dependence on the concentration / number of substitute elements of which overview is shown in Fig. 13 in Appendix. Motivated by our sample used in the neutron diffraction experiment, let us fix $n + l' = 0.2$ as a working cross section in the multi-dimensional composition space. Then the trade-off problem within this scope can be illustrated by comparing the plots, $Z_{\Delta E}(l)$ and $Z_M(l)$, as shown in Fig. 6. The conflicting trends between formation energy and magnetization reaches a compromise in the middle around $0.5 \leq l \leq 0.6$ as seen with the product $\tilde{U}_{\Delta E}(l)\tilde{U}_M(l)$ shown in Fig 7. In $\tilde{U}_{\Delta E} \equiv U_{\Delta E}(l) + 1.6$ and $\tilde{U}_M \equiv U_M(l) + 0.2$, an offset number has been incorporated into each target function so that all factors would be positive definite and a place to control external preference for prioritizing some of the observables can be reserved. The same procedure is applied to the target function whenever negative sign appears in the working space. Presence of such constants in order to have positive definite weights can be justified when the main interest lies in the relative trends among the target functions. There might be a better way to define the derivative coefficient in such a way that it is always positive definite by construction and introduce the external factors separately. At this stage the overall trend toward the optimal point is reasonable, in the sense that a combination of a increasing merit and a decreasing merit ends up with a best compromise in between. The procedure here is

(a)



(b)

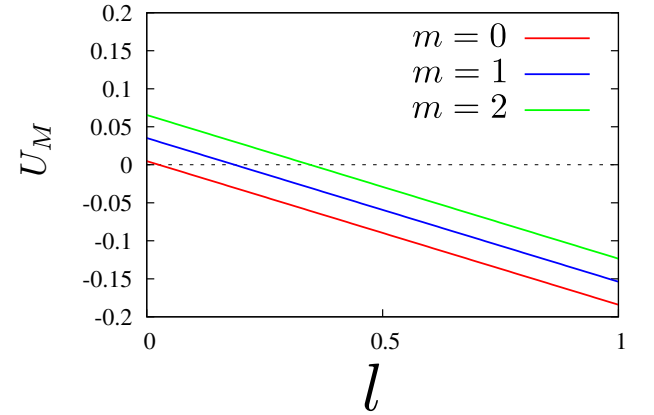


FIG. 6. (Color online) Utility of the target material Sm_{1-n}Zr_nFe_{12-m-l-l'}Co_mTi_lZr_{l'} as a function of l , with $n = 0.2$ and $l' = 0$ fixed.

partly in an analogy to adding a constant to the diagonal elements of density matrices involved in quantum Monte Carlo methods³⁶ in order to define positive definite weights. Thus redefined target function is denoted by \tilde{U} . We note that the best compromise always comes with more than 0.5 Ti atoms in the currently working cross section, in agreement with the past experimental findings^{15,16,18}.

It is the dimensionless parameter set as defined in Eq. (3) that enables the combination of observables with different dimensions, such as the product $\tilde{U}_{\Delta E}(l)\tilde{U}_M(l)$ as demonstrated above. Multiple requirements are often simultaneously imposed on practical materials, even to the level where non-physical or extrinsic requirements, such as environmental friendliness or prices of ingredient elements, need to be incorporated with some parametriza-

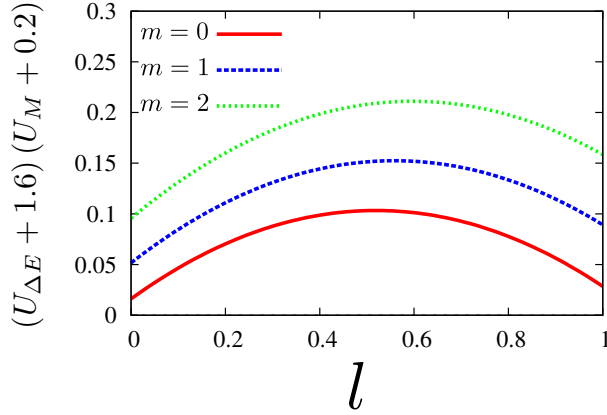


FIG. 7. (Color online) Compromise between structure stability and magnetization inspected with the partial utility functions of the target material $\text{Sm}_{1-n}\text{Zr}_n\text{Fe}_{12-m-l-l'}\text{Co}_m\text{Ti}_l\text{Zr}_{l'}$ as a function of l , with $n = 0.2$ and $l' = 0$ fixed.

tion in order to implement a multiple-objective optimization. What is implemented here constitutes a starting point of such comprehensive optimization framework for materials design. Equation (3) may not be the unique way to formulate the dimensionless parameters but we would consider that this can be one of the most natural ways in the spirit of constructing a manifold in the general materials space. More mathematically rigorous construction might be possible. As a crude starting point, the overall optimization can be inspected with an overall utility function as we can define as follows

$$U_{\text{all}} \equiv \tilde{U}_{\Delta E} \tilde{U}_M \tilde{U}_{T_c} \tilde{U}_{J_{\text{RT}}(8f)} \tilde{U}_{J_{\text{RT}}(8i)} \tilde{U}_{J_{\text{RT}}(8j)}$$

for which the data within the working cross-section on $n = 0.2$ and $l' = 0$ are shown in Fig. 8 for a few choices of the number of substituted Co atoms. The amount of Ti around 0.5 in the overall optimization problem seems to be a dead-end within the present working space.

IV. DISCUSSIONS

A. Toward more optimal materials

The lower bound identified for the amount of Ti in the ferromagnet based on the ThMn_{12} structure seems to be consistent with what has been established by experimental efforts in the past three decades^{13,14,17,21}. In principle our methodology can predict the limiting case to save a lot of those experimental efforts. This is going to be a help in the upcoming development of new materials with multiple relevant observables for a given utility. Given that 0.5 Ti atoms per formula unit seems to be the best compromise with SmFe_{12} for permanent-magnet utility,

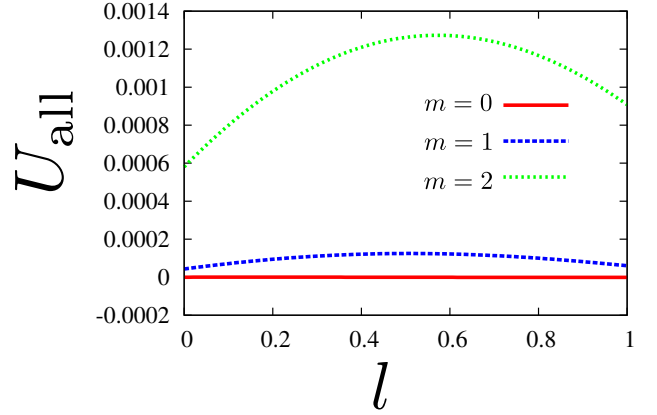


FIG. 8. (Color online) Compromise between structure stability, magnetization, Curie temperature, and room-temperature anisotropy field of which leading-order trend may be well captured by Sm-Fe exchange couplings. Overall product of the partial utility functions for the target material $\text{Sm}_{1-n}\text{Zr}_n\text{Fe}_{12-m-l-l'}\text{Co}_m\text{Ti}_l\text{Zr}_{l'}$ as a function of l , with $n = 0.2$ and $l' = 0$ fixed.

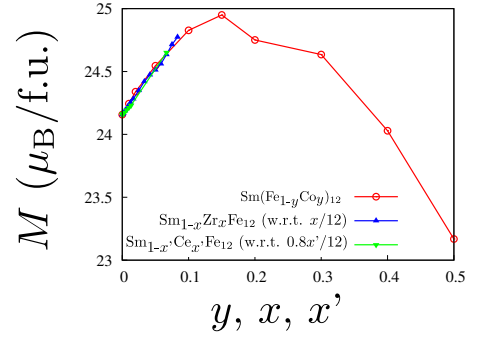


FIG. 9. (Color online) Calculated magnetization of doped SmFe_{12} per formula unit (f.u.) on a fixed lattice of SmFe_{12} ²³. It is seen that one extra electron from $\text{Zr}(2a)$ or $\text{Ce}(2a)$, with a proper rescaling of the concentration on the horizontal axis, works like one more electron in the minority spin band from Co and an analogue of the Slater-Pauling curve can be realized in the doped $2a$ site.

the working space needs to be extended in order to go beyond what has been achieved so far.

Furthermore, our formulation can straightforwardly incorporate more information including lattice-structure variants and external requirements on each element as long as they can be sufficiently well parametrized. Not only concerning the intrinsic properties of the target materials, but also various external factors could also be optimized altogether to design a good working bulk material.

B. Enhancing magnetization in SmFe_{12} by substitution

Calculated magnetization for partly substituted SmFe_{12} is summarized in Fig. 9 which show the celebrated Slater-Pauling curve^{37,38} for $\text{Sm}(\text{Fe},\text{Co})_{12}$. Remarkably, partly substituting $\text{Sm}(2a)$ by Zr shows analogous enhancement of magnetization which is demonstrated in Fig. 9 by a proper rescaling of the concentration of substitute elements. Experimentally, it might be counter-intuitive to see an enhancement of magnetization triggered by non-magnetic elements like Zr, while we argue below that this trend can be naturally interpreted in terms of electron number counting. The mechanism is attributed to charge transfer from $\text{Zr}(2a)$ to $\text{Fe}(8f)$. The same mechanism holds for $\text{Ce}^{4+}(2a)$ where the delocalized $4f$ -electron gets transferred to $\text{Fe}(8f)$.

1. Slater-Pauling curve in $\text{Sm}(\text{Fe},\text{Co})_{12}$

Calculated density of states for SmFe_{12} in Fig. 14 shown in Appendix points to a key role carried by $\text{Fe}(8f)$ sublattice in realizing the Slater-Pauling curve. When a part of the majority spin band of Fe has an overlap on the Fermi level, partial substitution of Fe by Co leads to the electronic state where the majority-spin state gets shifted toward below the Fermi level, enhancing the intrinsic magnetization^{39–43}. In Fig. 14, majority-spin state overlapping the Fermi level is mostly carried by $\text{Fe}(8f)$ and thus $\text{Fe}(8f)$ seems to be dominantly involved in the observed Slater-Pauling curve in Fig. 9, even though the substituting Co has been put uniformly over all of the Fe sublattices without caring for the relatively minor site preference. We note in passing that the Nd-analogue, NdFe_{12} as was investigated in Ref. 6, does not have much of the majority-spin states overlapping the Fermi level and thus would not show the Slater-Pauling curve for magnetization. The difference comes from the smaller lattice constant of the present Sm variant.

2. Electron doping into $\text{Fe}(8f)$ by substituted Zr in $\text{Sm}(2a)$

We observe that $\text{Zr}(2a)$ actually helps in enhancing magnetization and other observables in partly substituted SmFe_{12} , instead of diluting the magnetic properties of pristine SmFe_{12} , within the approximation of the fixed lattice. Care must be taken in assessing the nature of the electronic states of intermetallics where a significant part of the electrons are delocalized, and naive expectation such as dilution of magnetic moments which is rather oriented for a qualitative picture of insulators may not hold in some cases. It is seen in the calculated density of states for ZrFe_{12} in Figs. 15 (a), (b) and (c) shown in Appendix that delocalized $4d$ -electron states from Zr in ZrFe_{12} contributes like Co, in that both of Co and $\text{Zr}(2a)$ reduce the overlap of the majority-spin states on the Fermi level for

$\text{Fe}(8f)$. Thus the Slater-Pauling curve with Co adding up one electron on top of $3d$ -electron band of Fe, most significantly $\text{Fe}(8f)$, to maximize the magnetization can be simulated with $\text{Zr}(2a)$ also adding up electron via the delocalized $4d$ -electrons. The magnetic equivalent of Zr to Co is measured by a rescaling $12x \simeq y$ as can be inspected in Fig. 9. Here the intersite distance between $\text{Sm}(2a)$ and $\text{Fe}(8f)$ of the host lattice seems to fall in a good range in realizing the charge transfer from $\text{Zr}(2a)$ to $\text{Fe}(8f)$.

3. Electron doping into $\text{Fe}(8f)$ by substituted Ce^{4+}

Having seen the positive impact of $\text{Zr}(2a)$ in SmFe_{12} , the same effect can be expected for Ce^{4+} substituting the $\text{Sm}(2a)$ site in providing the additional electron with the delocalized $4f$ electron. A part of the delocalized $4f$ -electrons, which seems to be 80% as inspected from a manual scaling to achieve the data collapse seen in Fig. 9, hybridizes with d -electron band and adds up the filling, leading to an analogue of the Slater-Pauling curve in the particular electronic structure with the charge transfer from $\text{Ce}^{4+}(2a)$ to $\text{Fe}(8f)$.

Further details are given in Sec. D in Appendix.

V. CONCLUSIONS AND OUTLOOK

We have inspected an optimal chemical composition for a ferromagnet SmFe_{12} presuming the possible utility as a permanent magnet. Representative substitute elements, Ti, Co, Zr have been considered. Combining experimental data and *ab initio* data in a self-consistent way, we have seen that, in Zr-substituted SmFe_{12} , Zr occupies both $\text{Sm}(2a)$ and $\text{Fe}(8i)$ almost equally likely in terms of energetics. While Ti as the stabilization element has been found to be unavoidable, the lower bound found *ab initio* around 0.5 is close to what has been achieved experimentally so far²⁰.

Concerning the intrinsic magnetization enhanced by Zr^{21} , we find that the electron doping effects brought by Zr can be exploited to gain both of structure stability and magnetization. The similar effect is expected for Ce as well. Both of these happens because of the particular electronic structure with the hybridization between $3d$ -electron band from the Fe sublattices and $5d$ -electron band from rare earth sublattice.

Methodologically, the construction to iterate between macroscopically measured experimental data and microscopically calculated *ab initio* data might make a step forward to a multi-scale description of materials, which should be an important part of the possible theoretical description of coercivity of REPM's.

ACKNOWLEDGMENTS

This work is partly supported by JST-Mirai Program, Grant Number JPMJMI19G1, and is partly supported by the Elements Strategy Initiative Center for Magnetic Materials (ESICMM), Grant Number 12016013, through the Ministry of Education, Culture, Sports, Science and Technology (MEXT). We gratefully acknowledge the financial support by Toyota Motor Corporation. The sample preparation was performed under the future pioneering program Development of magnetic material technology for high-efficiency motors commissioned by the New Energy and Industrial Technology Development Organization (NEDO), Japan. Part of this work was performed at Australian Nuclear Science and Technology Organisation (ANSTO), and J. R. Hester's help in the collection of experimental data is gratefully acknowledged. One of the authors (MM) gratefully acknowledges helpful discussions with M. Ito, N. Sakuma, M. Yano, T. Shoji, T. Miyake, Y. Harashima, T. Ozaki, H. Akai, M. Hoffmann, C. E. Patrick, J. B. Staunton in related projects. He also benefited from comments and suggestions given by Y. Kuramoto, K. Ohashi, S. Sakurada, X. Tang, G. Hrkac, T. Ishikawa. Numerical computations were executed on System B in ISSP Supercomputer Center, University of Tokyo. Images in Figs. 1 and 3 have been generated using CrystalMaker[®]: a crystal and molecular structures program for Mac and Windows. CrystalMaker Software Ltd, Oxford, England (www.crystallmaker.com).

Appendix A: Details of *ab initio* calculations

1. *Ab initio* structure optimization of stoichiometric compounds and compounds on discrete points in chemical composition space

The structure optimization has been done utilizing the open-source package for *ab initio* electronic structure calculations, OpenMX^{44–49} which works on the basis of pseudopotentials^{50,51} and localized basis sets. Present type of *ab initio* structure optimization utilizing OpenMX to evaluate the formation energy referring to elemental systems have been described elsewhere⁵². We concisely describe what is extensively used in the present study. The choice of the local basis set has been the followings: Sm8.0-0C-s2p2d2f1, Fe6.0S-s2p2d1, Co6.0S-s2p2d2f1, Ti7.0-s3p3d3f1, and Zr7.0-s3p3d3f1, within the generalized gradient approximation (GGA) according to Perdew, Burke, and Ernzerhof (PBE)²². Partial core correction in the open-core approximation for Sm is set both for α -Sm as the reference system and the target compound SmFe₁₂. Convergence with respect to the number of *k*-points and the

cutoff energy is monitored. Given a material M, the optimized structure comes with the calculated energy on the basis of the choice of the particular basis set as given

M	$N_{\text{atom}}[\text{M}]$	U_{tot} (eV)
hcp-Ti	2	−3227.8
hcp-Zr	2	−2634.5
bcc-Fe	1	−2437.4
hcp-Co	2	−5830.3
α -Sm	9	−11383

TABLE III. Calculated energy for the reference elemental systems based on the local basis sets as described in the text. The data for bcc-Fe, hcp-Co, and α -Sm are taken from Ref. 52 and reproduced here for the convenience of reference.

above: we will refer to this calculated energy as “ $U_{\text{tot}}[\text{M}]$ ” for the convenience of reference. We note that U_{tot} has been defined up to the particular choice of the basis sets and the pseudopotentials specified above and it is not entirely the true total energy.

In the lattice structure of SmFe₁₂ shown in Fig. 1 in the main text, there are three sublattices for Fe, namely, Fe(8*i*), Fe(8*j*), and Fe(8*f*), and one rare-earth sublattice, Sm(2*a*). The internal cartesian coordinates of them can be defined as Sm(2*a*)(0,0,0), Fe(8*i*)(x_i ,0,0), Fe(8*j*)(x_j ,0.5,0), and Fe(8*f*)(0.5 − x_{8j} ,0,0.5). It is instructive to note that Fe(8*i*) and Fe(8*j*) atoms approximately form a regular hexagon, corresponding to Co(2*c*) atoms in the SmCo₅ prototype⁵⁵ on the side faces of the tetragonal box shown in Fig. 1 of the main text. There is a relation $2(0.5 - x_i) \simeq x_j$ among the internal coordinates as imposed by the local hexagonal symmetry of the CaCu₅ prototype. We typically set a set of starting internal coordinates, (x_{8i}, x_{8j}) = (0.36, 0.27) which roughly satisfies this relation. Referring to the recent experimental work on NdFe₁₂⁷ we set a set of starting lattice constants to be (a, c) = (8.52, 4.80) (Å). With these starting structure parameters, one of the host atoms in the tetragonal unit, with two formula units i.e. two Sm atoms and 24 Fe atoms, are replaced by substitute atoms one by one, and the crystal lattice structure is optimized to evaluate the total energy of the electronic state with the given chemical composition. For Zr-substituted SmFe₁₂, we obtain the optimized lattice parameters for each of (Sm,Zr)Fe₂₄ and Sm₂Fe₂₃Zr on the tetragonal unit with two formula units and compare the relative trends among them concerning magnetization and the energy of the electronic state.

The formation energy $\Delta E[\text{C}]$ of a compound C is defined as a difference between the energy of the compound and the sum of the energy of the constitute elemental systems as follows:

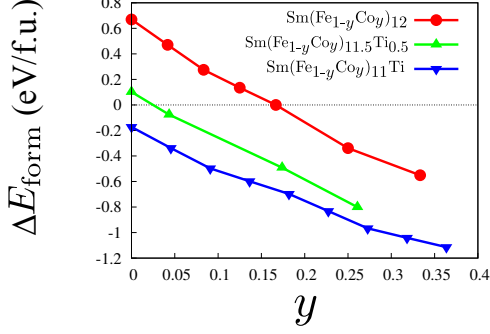


FIG. 10. (Color online) Calculated formation energy of Co-substituted SmFe_{12} , $\text{SmFe}_{11.5}\text{Ti}_{0.5}$, and $\text{SmFe}_{11}\text{Ti}$ per formula unit (f.u.). The reference systems are the ingredient elements.

$$\begin{aligned} \Delta E_{\text{form}}[\text{Sm}_{1-x}\text{Zr}_x(\text{Fe}_{1-y-z}\text{Co}_y\text{Ti}_z)_{12}] \\ \equiv U_{\text{tot}}[\text{Sm}_{1-x}\text{Zr}_x(\text{Fe}_{1-y-z}\text{Co}_y\text{Ti}_z)_{12}] - (1-x)\frac{U_{\text{tot}}[\alpha\text{-Sm}]}{N_{\text{atom}}[\alpha\text{-Sm}]} - x\frac{U_{\text{tot}}[\text{hcp-Zr}]}{N_{\text{atom}}[\text{hcp-Zr}]} \\ - 12(1-y-z)\frac{U_{\text{tot}}[\text{bcc-Fe}]}{N_{\text{atom}}[\text{bcc-Fe}]} - 12y\frac{U_{\text{tot}}[\text{hcp-Co}]}{N_{\text{atom}}[\text{hcp-Co}]} - 12z\frac{U_{\text{tot}}[\text{hcp-Ti}]}{N_{\text{atom}}[\text{hcp-Ti}]} \end{aligned} \quad (\text{A1})$$

Here $N_{\text{atom}}[\alpha\text{-Sm}] = 9$, $N_{\text{atom}}[\text{hcp-Zr}] = 2$, $N_{\text{atom}}[\text{bcc-Fe}] = 1$, $N_{\text{atom}}[\text{hcp-Co}] = 2$, and $N_{\text{atom}}[\text{hcp-Ti}] = 2$, are the number atoms in the unit cell of the elemental systems. Calculated results for the formation energy of Co-substituted SmFe_{12} , $\text{SmFe}_{11.5}\text{Ti}_{0.5}$, and $\text{SmFe}_{11}\text{Ti}$ with respect to the concentration of Co are shown in Fig. 10. Referring to Fig. 2 in the main text and results of previous works, we have selectively put Ti in the $\text{Fe}(8i)$ sublattice and Co in the $\text{Fe}(8f)$ sublattice in order to get the overall trend of the formation energy with respect to the concentration of substituted Co. It is again confirmed that SmFe_{12} substituted with Ti significantly gains the formation energy. Also the presence of Co helps the formation energy to be negative and large: Co substitution in SmFe_{12} can be the rare case where

both of the strong ferromagnetism and structure stability can be gained at the same time, as long as possible other compounds with different crystal structure do not compete severely in the formation.

In the present case of the assessment of formation of SmFe_{12} , the most probable competing phase would be $\text{Sm}_2\text{Fe}_{17}$. The crystal structure of $\text{Sm}_2\text{Fe}_{17}$, of the rhombohedral type belonging to the Space Group No. 166, is common among $4f\text{-}3d$ intermetallic compounds in REPM's, such as $\text{Sm}_2\text{Co}_{17}$ in the main cell phase of the Sm-Co magnet⁵³ that was the champion magnet in 1970's and $\text{Sm}_2\text{Fe}_{17}\text{N}_x$ that has been a candidate since early 1990's to potentially go beyond $\text{Nd}_2\text{Fe}_{14}\text{B}$ -based REPM⁵⁴. A relative formation energy of SmT_{12} referring to Sm_2T_{17} ($\text{T}=\text{Fe}$ or Co), $\Delta E_{\text{form}}^{\text{relative}}$, can be defined as follows,

$$\Delta E_{\text{form}}^{\text{relative}}[\text{SmFe}_{12}] \equiv \frac{U_{\text{tot}}[\text{SmFe}_{12}]}{N_{\text{fu}}[\text{SmFe}_{12}]} - \frac{1}{2}\frac{U_{\text{tot}}[\text{Sm}_2\text{Fe}_{17}]}{N_{\text{fu}}[\text{Sm}_2\text{Fe}_{17}]} - \frac{7}{2}\frac{U_{\text{tot}}[\text{bcc-Fe}]}{N_{\text{atom}}[\text{bcc-Fe}]} \quad (\text{A2})$$

and

$$\Delta E_{\text{form}}^{\text{relative}}[\text{SmCo}_{12}] \equiv \frac{U_{\text{tot}}[\text{SmCo}_{12}]}{N_{\text{fu}}[\text{SmCo}_{12}]} - \frac{1}{2}\frac{U_{\text{tot}}[\text{Sm}_2\text{Co}_{17}]}{N_{\text{fu}}[\text{Sm}_2\text{Co}_{17}]} - \frac{7}{2}\frac{U_{\text{tot}}[\text{hcp-Co}]}{N_{\text{atom}}[\text{hcp-Co}]} \quad (\text{A3})$$

Thus defined relative formation energy of doped SmFe_{12} referring to $\text{Sm}_2\text{Fe}_{17}$ is shown in Fig. 11. Compared to

the data in Fig. 2 in the main text, Zr in $\text{Fe}(8i)$ looks more energetically favorable than being in $\text{Sm}(2a)$ sub-

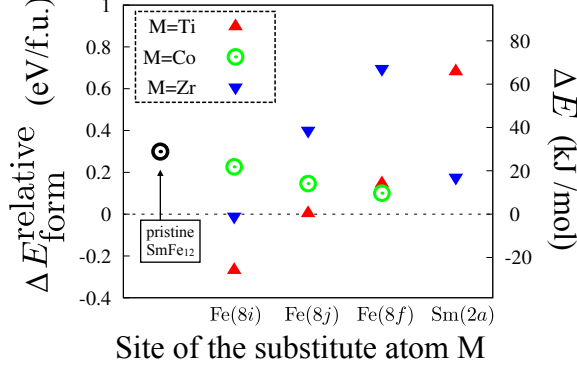


FIG. 11. (Color online) Calculated formation energy of M-substituted SmFe_{12} ($M=\text{Ti}$, Co , and Zr) per formula unit (f.u.). The reference system is taken to be $\text{Sm}_2\text{Fe}_{17}$ in the same spirit as is written in Eq. (A2). The same data as those shown in Fig. 2 in the main text are plotted with the reference systems set to be $\text{Sm}_2\text{Fe}_{17}$.

M	$U_{\text{tot}}[M]$ (eV)	$N_{\text{fu}}[M]$
SmFe_{12}	-61026	2
SmCo_{12}	-72494	2
$\text{Sm}_2\text{Fe}_{17}$	-43965	1
$\text{Sm}_2\text{Co}_{17}$	-52089	1

TABLE IV. Calculated energy with the optimized structure for the target compounds SmFe_{12} and SmCo_{12} and the corresponding data for the reference systems $\text{Sm}_2\text{Fe}_{17}$ and $\text{Sm}_2\text{Co}_{17}$, respectively. Number of formula units in the optimized structure is denoted as N_{fu} .

lattice. On the basis of *ab initio* electronic structure of doped SmFe_{12} , we do not see any particular reason to expect that Zr would be selectively substituting the $\text{Sm}(2a)$ site except for the possible scenario that Ti and Zr compete over the most preferable $\text{Fe}(8i)$ sites and Ti atoms dominate with the larger energy gain than Zr atoms. As a compromise, Zr atoms can go more into $\text{Sm}(2a)$ sites than into $\text{Fe}(8i)$ sites.

It is indeed true that the relative formation energy of SmT_{12} referring to Sm_2T_{17} is slightly lower for the $\text{T}=\text{Co}$ case, but still both stoichiometric limits of SmT_{12} ($\text{T}=\text{Fe}$ or Co) will be purged by the formation of Sm_2T_{17} because the latter is more favorable energetically. Thus the decreasing slope on the Co concentration axis seen in Fig. 10 does not straightforwardly point to a true gain in the structure stability when the intervening phases such as $\text{Sm}_2\text{Co}_{17}$ comes in. At least in the middle of Fe-Co

axis, most promising chemical composition concerning the stability is seen on a slightly Fe-rich side as we explore the chemical composition space continuously as described below.

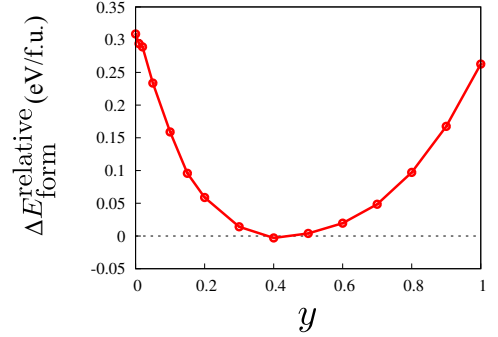


FIG. 12. (Color online) Interpolated formation energy of SmT_{12} per formula unit (f.u.) with the reference systems being $\text{Sm}_2\text{Fe}_{17}$ and $\text{Sm}_2\text{Co}_{17}$ following Eqs. (A2), (A3), (A4), and (A5).

2. *Ab initio* interpolation for alloys

Fractional parameters of the chemical composition can be continuously explored with coherent potential approximation (CPA) for random alloys. Korringa-Kohn-Rostoker (KKR)⁵⁶ Green's function method combined with CPA (KKR-CPA) provides a convenient way to obtain an interpolated electronic structure, e.g. for $\text{Sm}(\text{Fe}_{1-y}\text{Co}_y)_{12}$ with $0 < y < 1$, between the stoichiometric limits of SmFe_{12} and SmCo_{12} . We have used the implementation of KKR-CPA in AkaiKKR⁵⁷.

KKR-CPA can yield a reliable estimate of magnetization and magnetic exchange couplings for magnetic alloys as a continuous function of the composition parameters. Unfortunately, the absolute value of calculated energy, which we denote here by $E_{\text{tot}}^{\text{KKRCPA}}$, suffer from a systematic deviation due to a cutoff parameter l_{max} in the expansion with respect to spherical harmonics in solving the multiple scattering problem at the core of KKR Green's function method. In the present calculations we set $l_{\text{max}} = 2$ for all elements which should be well justified within the open-core approximation assuming well localized $4f$ -electrons. Comparison of calculated energy between different materials can be tricky within KKR-CPA but it is feasible to observe the trend in the calculated energy as long as the range of the target materials is restricted within the same type of crystal structure. Thus mixing energy ΔE_{mix} of an alloy defined in Eq. (A4) below can be combined with the formation energy calculated for the stoichiometric compounds to assess an interpolated formation energy for alloys.

$$\Delta E_{\text{mix}}[\text{Sm}(\text{Fe}_{1-x}\text{Co}_x)_{12}]$$

$$\equiv E_{\text{tot}}^{\text{KKRCPA}}[\text{Sm}(\text{Fe}_{1-x}\text{Co}_x)_{12}] - (1-x)E_{\text{tot}}^{\text{KKRCPA}}[\text{SmFe}_{12}] - xE_{\text{tot}}^{\text{KKRCPA}}[\text{SmCo}_{12}] \quad (\text{A4})$$

Combining the formation energy for the stoichiometric compounds and the mixing energy for alloys, an interpolated formation energy for the alloy can be estimated as follows:

$$\Delta E_{\text{form}}^{\text{relative}}[\text{Sm}(\text{Fe}_{1-x}\text{Co}_x)_{12}] \simeq (1-x)\Delta E_{\text{form}}^{\text{relative}}[\text{SmFe}_{12}] + \Delta E_{\text{mix}}[\text{Sm}(\text{Fe}_{1-x}\text{Co}_x)_{12}] + x\Delta E_{\text{form}}^{\text{relative}}[\text{SmCo}_{12}] \quad (\text{A5})$$

The results for $\text{Sm}(\text{Fe}_{1-y}\text{Co}_y)_{12}$ are shown in Fig. 12. It is seen that 40% of Co can bring the formation energy of the 1:12 phase almost on a par with the formation energy of 2:17 phase.

Appendix B: Details of the “LDA+Rietveld” iterations

Rietveld refinement of the neutron diffraction data for $\text{Sm}_{0.8}\text{Zr}_{0.2}(\text{Fe}_{0.7}\text{Co}_{0.3})_{11.25}\text{Ti}_{0.75}$ has been done utilizing the FullProf program⁵⁸. AkaiKKR⁵⁷ was employed to calculate the magnetic moments of each atom from first principles with the lattice structure information provided by Rietveld analysis as the input. Then the output of AkaiKKR for calculated magnetic moments is fed back to the Rietveld analysis in the next stage, and the overall process is iterated until the parameters in the inputs and the outputs converge.

It is to be noted that the experimental measurements are done at room temperature and *ab initio* calculations are done at zero temperature. Since our Co-containing samples come with sufficiently high Curie temperatures beyond 800K⁵⁹, we regard that room temperature is close enough to zero temperature for the present analysis. If the Curie temperature of the sample is not quite high, we would turn to *ab initio* finite temperature calculations formulated on the basis of KKR-CPA^{60–66} at the cost of some extra computational time. For Co-substituted SmFe_{12} , we can safely skip this.

Remarkably, the convergence of the overall LDA+Rietveld iteration is achieved within only a few iteration steps as are shown in Table V with the input and output parameters of KKR-CPA. Here we count a set of Rietveld analysis and *ab initio* calculation as one iteration step. We observe that either $\text{Sm}(2a)$ or $\text{Fe}(8i)$ can accommodate the Zr atoms in an equally plausible way. Thus the message from the data from the *ab initio* structure optimization for the site preference of Zr is confirmed in the analysis of the neutron diffraction data for the real sample, $\text{Sm}_{0.8}\text{Zr}_{0.2}(\text{Fe}_{0.75}\text{Co}_{0.25})_{11.25}\text{Ti}_{0.75}$. Details of the Rietveld analysis together with a wider range of target compounds will be reported elsewhere⁶⁷.

Appendix C: Extracting the derivative of the target observables with respect to the chemical composition parameters

On a fixed lattice of SmFe_{12} ²³, we inspect the derivative of the target observables as a function of the chemical composition parameters, namely, x , y , z , and z' in $(\text{Sm}_{1-x}\text{Zr}_x)(\text{Fe}_{1-y-z/3-z'/3}\text{Co}_y\text{Ti}_{z/3}\text{Zr}_{z'/3})_{12}$. Here, x denotes the concentration of the substitute element within the $\text{Sm}(2a)$ sublattice, y does the concentration of the substitute element on the overall Fe sublattice, and z/z' denote the concentration of the substitute element within the $\text{Fe}(8i)$ sublattice. They are not to be confused with the notation in Sec. A 1 used in order to illustrate the definition of the formation energy. Relating to the number of substitute elements per formula unit n , m , l , and l' in $\text{Sm}_{1-n}\text{Zr}_n\text{Fe}_{12-m-l-l'}\text{Co}_m\text{Ti}_l\text{Zr}_{l'}$, the following relations hold:

$$\begin{aligned} n &= x, \\ m &= 12y, \\ l &= 4z, \\ l' &= 4z'. \end{aligned}$$

Fixed-lattice approximation has been employed here on the assumption that chemical composition i.e. the variation in the electron number affects the intrinsic properties more significantly than the variation in the lattice parameters does as long as the linear extrapolation around a reasonable stoichiometric limit²³ is attempted. Also the effect of the celebrated Slater-Pauling curve can be more easily demonstrated with the smaller lattice constants. Thus the smaller *ab initio* parameter set from Table I in the main text has been taken. The other parameter sets would yield the similar messages. The overall data can be glanced in Fig. 13. Here the point is to confirm the existence of the linear regime spanning a reasonable range around the pristine/stoichiometric limit in the chemical composition space. Then within such linear regime, we can discuss at which parameter range the target observables can be optimized on demand.

From the data shown in Fig. 13, the derivative of an observable \mathcal{O} around the pristine limit is obtained as a difference between $c = 0$ and $c = 0.01$, where $c = x, y, z$, or z' is the concentration of the substitute elements, and then multiplied by 100:

$$\frac{\partial \mathcal{O}}{\partial c} \equiv \frac{\mathcal{O}|_{c=0.01} - \mathcal{O}|_{c=0}}{0.01} \quad (\text{C1})$$

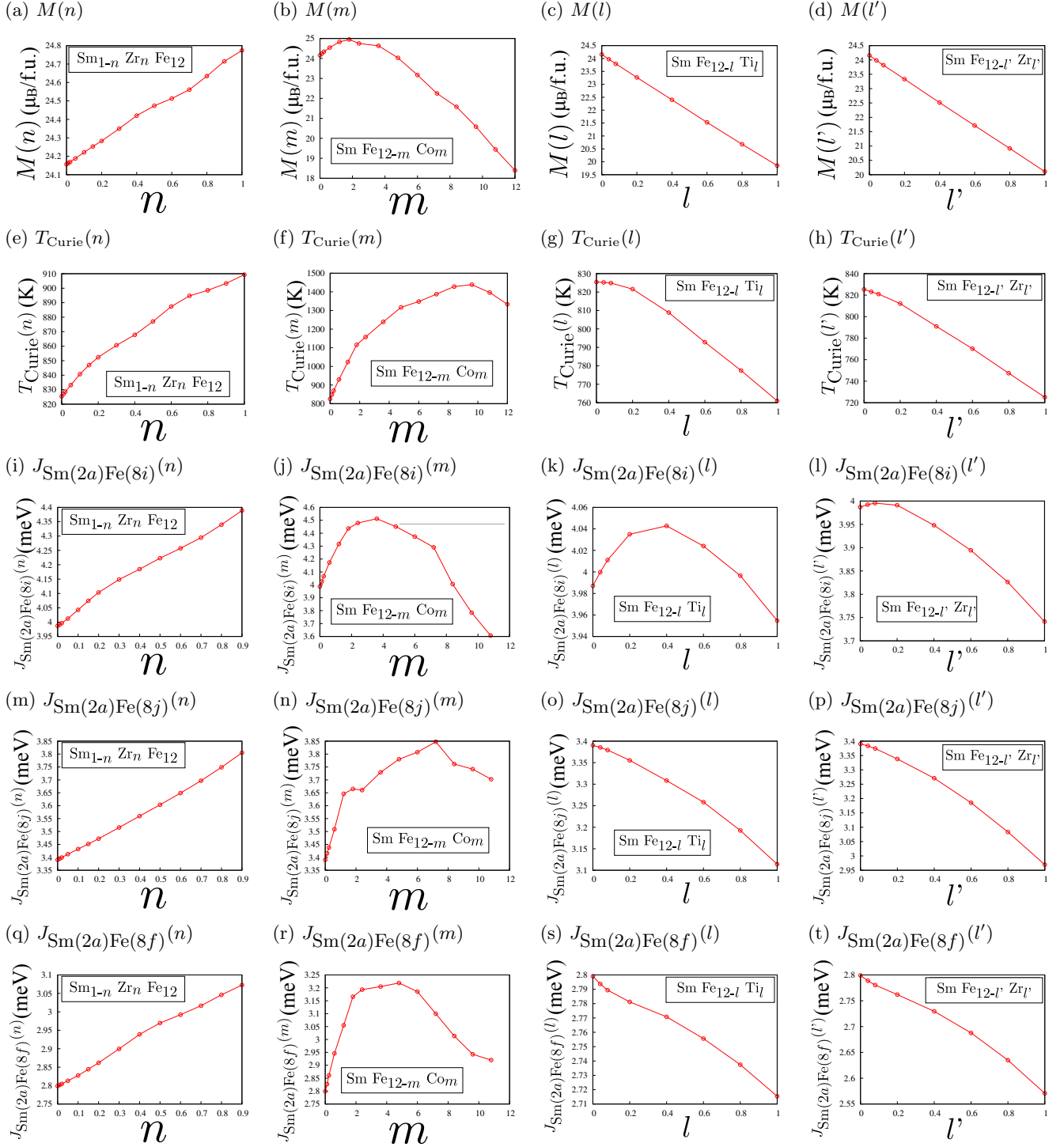


FIG. 13. Deriving the derivative matrix of the intrinsic properties for the target alloy, $\text{Sm}_{1-n}\text{Zr}_n(\text{Fe}_{12-m-l-l'}\text{Co}_m\text{Ti}_l\text{Zr}_{l'})$ around the pristine limit, SmFe_{12} , from the calculated data via KKR-CPA using AkaiKKR. Dependence of magnetization M per formula unit (f.u.), Curie temperature T_{Curie} , and Sm-Fe indirect exchange couplings J_{RT} for $\text{Fe}(8i)$, $\text{Fe}(8j)$, $\text{Fe}(8f)$ that are crucial for anisotropy field in the operation temperature range, are plotted with respect to the concentration of substitute elements, Zr, Co, and Ti. For Zr two possible substitution sublattices, $\text{Sm}(2a)$ and $\text{Fe}(8i)$, are explored.

(a) Zr in Sm(2a)

KKR-CPA	step 1		step 2		step 3	
	inputs	outputs (μ_B)	inputs	outputs (μ_B)	inputs	outputs (μ_B)
8f Fe	69.2%	1.89946	70.4%	1.89762	70.4%	1.89768
Co	30.8%	1.32717	29.6%	1.32660	29.6%	1.32665
8i Fe $x_i = 0.35617$	73.6%	2.50941	$x_i = 0.35619$	72.4%	$x_i = 0.3562$	72.4%
Co	8%	1.66443	8.8%	1.66101	8.8%	1.66083
Ti	18.8%	-0.75328	18.8%	-0.75300	18.8%	-0.75306
8j Fe $x_j = 0.27678$	68%	2.28426	$x_j = 0.27645$	68%	$x_j = 0.27644$	68%
Co	32%	1.47931	32%	1.47928	32%	1.47936
2a Sm	80%	-0.41385	80%	-0.41207	80%	-0.41197
Zr	20%	-0.41066	20%	-0.41000	20%	-0.40995
(a (Å), c/a) for the unit cell	(8.50758, 0.5607)	21.3041	(8.50705, 0.5607)	21.2733	(8.50705, 0.5607)	21.2732
Calculated energy (Ry)	-47793.09020		-47787.10120		-47787.10106	

(b) Zr in Fe(8i)

KKR-CPA	step 1		step 2		step 3	
	inputs	outputs (μ_B)	inputs	outputs (μ_B)	inputs	outputs (μ_B)
8f Fe	69.17%	1.82528	70.63%	1.82613	70.63%	1.82611
Co	30.83%	1.26294	29.37%	1.26432	29.37%	1.26431
8i Fe $x_i = 0.35515$	70%	2.52271	$x_i = 0.35532$	68.77%	$x_i = 0.35532$	68.77%
Co	6.324%	1.67340	7.51%	1.66825	7.51%	1.66809
Ti	18.577%	-0.71585	18.57%	-0.71660	18.577%	-0.71663
Zr	5.138%	-0.43412	5.138%	-0.43445	5.138%	-0.43446
8j Fe $x_j = 0.27717$	68.379%	2.23359	$x_j = 0.27685$	68.25%	$x_j = 0.27683$	68.25%
Co	31.621%	1.42782	31.75%	1.42873	31.75%	1.42880
2a Sm	100%	-0.40525	100%	-0.40270	100%	-0.40259
(a (Å), c/a) for the unit cell	(8.50758, 0.5607)	20.3790	(8.50705, 0.5607)	20.3529	(8.50705, 0.5607)	20.3527
Calculated energy (Ry)	-51311.90695		-51310.68873		-51310.68847	

TABLE V. Proceedings of the “LDA+Rietveld” iteration. (a) assuming that Zr resides in Sm(2a) and (b) Zr resides only in Fe(8i). We find that either assumption works on a par as long as the Rietveld analysis combined with *ab initio* KKR-CPA is concerned. We note that the absolute values of the calculated energy via KKR-CPA should not be compared between (a) and (b), but only within (a) or (b).

Numbers during such derivation of the derivative matrix in the main text are displayed in Table VI. Eventually they are translated into the derivative with respect to the number of substitute elements per formula unit and are summarized in Eq. (3) in the main text.

Appendix D: Slater-Pauling curve and electron-doping effect in SmFe₁₂

Co-substituted SmFe₁₂ on a fixed lattice of computational optimization²³ nicely shows the Slater-Pauling curve as shown in Fig. 13 (b). The origin of this can be tracked down to the residual density of states around

the Fermi level in the majority spin band as shown in Fig. 14. This contribution comes mostly from the Fe(8f) sublattice. With the introduction of Co, extra electrons are added in the minority spin band, and we have noted that the analogous effect is given by Zr and also by Ce substituting the Sm(2a) sublattice. As a comparison calculated density of states for ZrFe₁₂ and CeFe₁₂ are shown in Figs. 15 (a), (b), and (c) for the data projected onto the Fe(8f) atoms, Fe(8i), and Fe(8j), respectively. In Fig. 15 (a) it is seen that replacement of Sm with Zr or Ce has pushed down the majority-spin band down below the Fermi level, leading to the enhancement of magnetization.

Zr(2a)-induced enhancement of magnetization and the

(a) raw data

	pristine	$x = 0.01$	$y = 0.01$	$z = 0.01$	$z' = 0.01$
M ($\mu_B/\text{f.u.}$)	24.1568	24.1627	24.2445	23.9738	23.9853
T_{Curie} (K)	825.377	827.001	848.566	825.219	823.075
$J_{\text{RT}}(8f)$ (meV)	2.799074	2.801749	2.827002	2.793691	2.788702
$J_{\text{RT}}(8i)$ (meV)	3.986962	3.991619	4.025465	3.999788	3.992307
$J_{\text{RT}}(8j)$ (meV)	3.390305	3.394893	3.415285	3.385382	3.383555

(b) the derivatives defined as Eq. (C1)

c , the concentration of the substitute elements	x	y	z	z'
$\partial M/\partial c$ ($\mu_B/\text{f.u.}$)	0.59	8.77	-18.3	-17.15
$\partial T_{\text{Curie}}/\partial c$ (K)	162.4	2318.9	-15.8	-230.2
$\partial J_{\text{RT}}(8f)/\partial c$ (meV)	0.2675	2.7928	-0.5383	-1.0372
$\partial J_{\text{RT}}(8i)/\partial c$ (meV)	0.4657	3.8503	1.2826	0.5345
$\partial J_{\text{RT}}(8j)/\partial c$ (meV)	0.4588	2.498	-0.4923	-0.675

(c) Normalized derivatives

	x	y	z	z'
$(\partial M/\partial c)/M$	0.0244238	0.363045	-0.757551	-0.709945
$(\partial T_{\text{Curie}}/\partial c)/T_{\text{Curie}}$	0.196759	2.8095	-0.0191428	-0.278903
$[\partial J_{\text{RT}}(8f)/\partial c]/J_{\text{RT}}(8f)$	0.0955673	0.997759	-0.192314	-0.370551
$[\partial J_{\text{RT}}(8i)/\partial c]/J_{\text{RT}}(8i)$	0.116806	0.965723	0.321699	0.134062
$[\partial J_{\text{RT}}(8j)/\partial c]/J_{\text{RT}}(8j)$	0.135327	0.736807	-0.145208	-0.199097

(d) Normalized derivatives with respect to the substitute atom number per formula unit, as used in the main text

	$n \equiv x$	$m \equiv 12y$	$l \equiv 4z$	$l' \equiv 4z'$
$(\partial M/\partial p)/M$	0.0244238	0.0302537	-0.189388	-0.177486
$(\partial T_{\text{Curie}}/\partial p)/T_{\text{Curie}}$	0.196759	0.234125	-0.0047857	-0.0697258
$[\partial J_{\text{RT}}(8f)/\partial p]/J_{\text{RT}}(8f)$	0.0955673	0.0831466	-0.0480785	-0.0926378
$[\partial J_{\text{RT}}(8i)/\partial p]/J_{\text{RT}}(8i)$	0.116806	0.0804769	0.0804248	0.0335155
$[\partial J_{\text{RT}}(8j)/\partial p]/J_{\text{RT}}(8j)$	0.135327	0.0614006	-0.036302	-0.0497742

TABLE VI. Numbers for the calculated derivatives from finite difference around the pristine limit for $\text{Sm}_{1-x}\text{Zr}_x(\text{Fe}_{1-y-z/3-z'/3}\text{Co}_y\text{Ti}_{z/3}\text{Zr}_{z'/3})_{12}$, or equivalently, $\text{Sm}_{1-n}\text{Zr}_n(\text{Fe}_{12-m-l-l'}\text{Co}_m\text{Ti}_l\text{Zr}_{l'})$ obtained from the data presented in Fig. 13. In (d), the number of substitute atoms has been denoted by $p = n, m, l$, or l' .

same effect from Ce^{4+} mostly happens as an extra electron is doped in the minority-spin state on the $\text{Fe}(8f)$ sublattice indicates that charge-transfer from the $\text{Sm}(2a)$ site to the $\text{Fe}(8f)$ site is the key factor in realizing the analogous behavior to Slater-Pauling curve as a function of substitute elements in the $\text{Sm}(2a)$ sublattice. Here we note that substituted Ce^{4+} supplying extra electrons in the host system is apparently analogous to electron-doped cuprates^{68,69}. While the host system, which is a metal that is not so good in terms of electric conduction,

resides on the opposite side of the presumed Mott insulator for cuprates⁷⁰ in a virtual materials space harboring a metal-insulator transition⁷¹, doping seems to work on the localized part of the electronic state that seems to be actually common between our $4f$ - $3d$ intermetallic ferromagnets and doped Mott insulators.

Understanding and control of such local mechanism in the real space should help in implementing fortunate cases like Zr-substituted SmFe_{12} ²¹, where both magnetic ferromagnetism and structure stability can be gained at the same time.

¹ M. Sagawa, S. Fujimura, N. Togawa, H. Yamamoto, Y. Matsuura, New material for permanent magnets on a base of Nd and Fe, J. Appl. Phys. **55**, 2083 (1984).

² J. J. Croat, J. F. Herbst, R. W. Lee, F. E. Pinkerton, Pr-Fe and Nd-Fe-based materials: A new class of high-performance permanent magnets, J. Appl. Phys. **55**, 2078

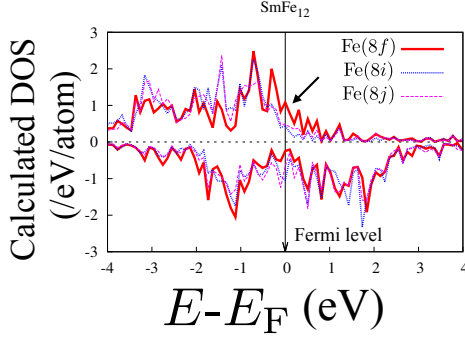


FIG. 14. (Color online) Calculated density of states (DOS) projected onto Fe atoms for the pristine SmFe_{12} on an optimized lattice²³. The horizontal axis shows the energy E as measured from the Fermi level, E_F . The arrow in the plot points to the extra density of states in the majority spin state projected onto $\text{Fe}(8f)$. Additional Co reduces this region leading to the Slater-Pauling curve.

(1984)

³ F. Spada, C. Abache, H. Oesterreicher, Crystallographic and magnetic properties of rare earth-transition metal compounds based on boron, *J. Less-Common Met.* **99**, L21 (1984).

⁴ For a review, see J. F. Herbst, $\text{R}_2\text{Fe}_{14}\text{B}$ materials: Intrinsic properties and technological aspects, *Rev. Mod. Phys.* **63**, 819 (1991).

⁵ For a review, see K. Hono and H. Sepehri-Amin, Strategy for high-coercivity Nd-Fe-B magnets, *Scr. Mater.* **67**, 530 (2012).

⁶ T. Miyake, K. Terakura, Y. Harashima, H. Kino, and S. Ishibashi, First-principles study of magnetocrystalline anisotropy and magnetization in NdFe_{12} , $\text{NdFe}_{11}\text{Ti}$, and $\text{NdFe}_{11}\text{TiN}$, *J. Phys. Soc. Jpn.* **83**, 043702 (2014).

⁷ Y. Hirayama, Y. K. Takahashi, S. Hirose, and K. Hono, $\text{NdFe}_{12}\text{N}_x$ hard-magnetic compound with high magnetization and anisotropy field, *Scr. Mater.* **95**, 70 (2015).

⁸ Y. Hirayama, T. Miyake, and K. Hono, Rare-earth lean hard magnet compound NdFe_{12}N , *JOM* **67**, 1344 (2015).

⁹ Y. Hirayama, Y. K. Takahashi, S. Hirose, and K. Hono, Intrinsic hard magnetic properties of $\text{Sm}(\text{Fe}_{1-x}\text{Co}_x)_{12}$ compound with the ThMn_{12} structure, *Scr. Mater.* **138**, 62 (2017).

¹⁰ K. Ohashi, T. Yokoyama, R. Osugi and Y. Tawara, The magnetic and structural properties of R-Ti-Fe ternary compounds, *IEEE Trans. Magn.* **23** 3101 (1987).

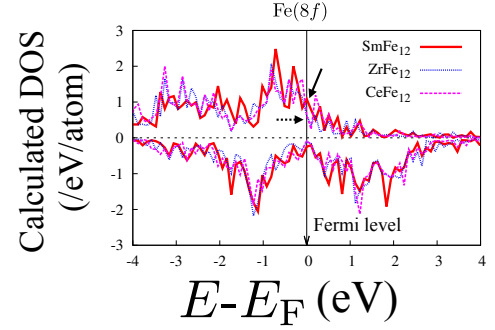
¹¹ For a recent review, see A. M. Gabay and G. C. Hadjipanayis, Recent developments in RFe_{12} -type compounds for permanent magnets, *Scr. Mater.* **154**, 284 (2018).

¹² G. C. Hadjipanayis, A. M. Gabay, A. M. Schönhöbel, A. Martín-Cid, J. M. Barandiaran, D. Niarchos, ThMn_{12} -Type Alloys for Permanent Magnets, *Engineering* **6**, 141 (2020).

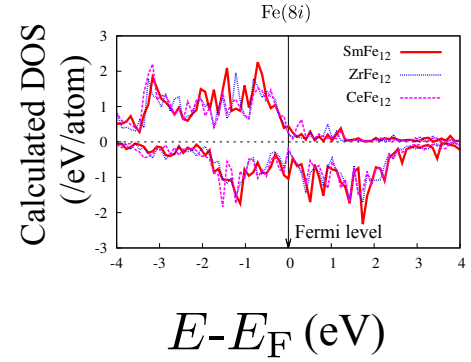
¹³ S. Sakurada, A. Tsutai, M. Sahashi, A study on the formation of ThMn_{12} and NaZn_{13} structures in $\text{RFe}_{10}\text{Si}_2$, *J. Alloys Compd.* **187**, 67 (1992).

¹⁴ S. Sakurada, A. Tsutai, T. Hirai, Y. Yanagida, M. Sahashi, S. Abe, and T. Kaneko, Structural and magnetic proper-

(a)



(b)



(c)

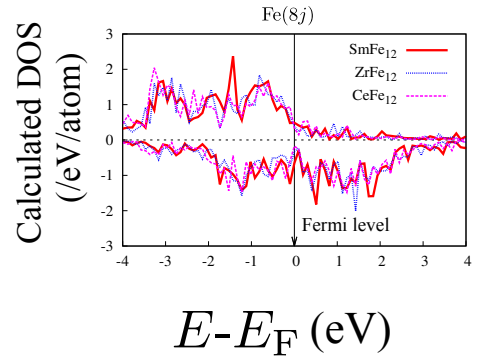


FIG. 15. (Color online) (a) Calculated density of states projected onto $\text{Fe}(8f)$ atoms for SmFe_{12} , ZrFe_{12} , and CeFe_{12} on the same fixed lattice. The full-line arrow in the plot points to the majority-spin density of states on the Fermi level which is seen significantly mostly for SmFe_{12} . Dotted arrow points to the relatively sparse contribution from the majority spin of $\text{Fe}(8f)$ in CeFe_{12} and ZrFe_{12} , which means that magnetic moments on $\text{Fe}(8f)$ are close to saturation for those materials. (b) and (c): Analogous data to (a) for $\text{Fe}(8i)$ and $\text{Fe}(8j)$, respectively. The axis labels follows them in Fig. 14.

- ties of rapidly quenched $(\text{R,Zr})(\text{Fe,Co})_{10}\text{N}_x$ ($\text{R}=\text{Nd, Sm}$), J. Appl. Phys. **79**, 4611 (1996).
- ¹⁵ S. Suzuki, T. Kuno, K. Urushibata, K. Kobayashi, N. Sakuma, K. Washio, H. Kishimoto, A. Kato, and A. Manabe, A $(\text{Nd,Zr})(\text{Fe,Co})_{11.5}\text{Ti}_{0.5}\text{N}_x$ compound as a permanent magnet material, AIP Advances **4**, 117131 (2014).
 - ¹⁶ S. Suzuki, T. Kuno, K. Urushibata, K. Kobayashi, N. Sakuma, K. Washio, M. Yano, A. Kato, A. Manabe, A new magnet material with ThMn_{12} structure: $(\text{Nd}_{1-x}\text{Zr}_x)(\text{Fe}_{1-y}\text{Co}_y)_{11+z}\text{Ti}_{1-z}\text{N}_\alpha$ ($\alpha = 0.6 - 1.3$), J. Magn. Magn. Mater. **401**, 259 (2016).
 - ¹⁷ N. Sakuma, S. Suzuki, T. Kuno, K. Urushibata, K. Kobayashi, M. Yano, A. Kato, and A. Manabe, Influence of Zr substitution on the stabilization of ThMn_{12} -type $(\text{Nd}_{1-\alpha}\text{Zr}_\alpha)(\text{Fe}_{0.75}\text{Co}_{0.25})_{11.25}\text{Ti}_{0.75}\text{N}_{1.2-1.4}$ ($\alpha = 0 - 0.3$) compounds, AIP Advances **6**, 056023 (2016).
 - ¹⁸ T. Kuno, S. Suzuki, K. Urushibata, K. Kobayashi, N. Sakuma, M. Yano, A. Kato, and A. Manabe, $(\text{Sm,Zr})(\text{Fe,Co})_{11.0-11.5}\text{Ti}_{1.0-0.5}$ compounds as new permanent magnet materials, AIP Advances **6**, 025221 (2016).
 - ¹⁹ M. Hagiwara, N. Sanada, S. Sakurada, Effect of Y substitution on the structural and magnetic properties of $\text{Sm}(\text{Fe}_{0.8}\text{Co}_{0.2})_{11.4}\text{Ti}_{0.6}$, J. Magn. Magn. Mater. **465**, 554 (2018).
 - ²⁰ P. Tozman, H. Sepehri-Amin, Y. K. Takahashi, S. Hirosawa, K. Hono, Intrinsic magnetic properties of $\text{Sm}(\text{Fe}_{1-x}\text{Co}_x)_{11}\text{Ti}$ and Zr-substituted $\text{Sm}_{1-y}\text{Zr}_y(\text{Fe}_{0.8}\text{Co}_{0.2})_{11.5}\text{Ti}_{0.5}$ compounds with ThMn_{12} structure toward the development of permanent magnets, Acta Materialia **153**, 354 (2018).
 - ²¹ P. Tozman, Y. K. Takahashi, H. Sepehri-Amin, D. Ogawa, S. Hirosawa, K. Hono, The effect of Zr substitution on saturation magnetization in $(\text{Sm}_{1-x}\text{Zr}_x)(\text{Fe}_{0.8}\text{Co}_{0.2})_{12}$ compound with the ThMn_{12} structure, Acta Materialia **178**, 114 (2019).
 - ²² J. P. Perdew, K. Burke, and M. Ernzerhof, Generalized Gradient Approximation Made Simple, Phys. Rev. Lett. **77**, 3865 (1996); *ibid* **78**, 1396 (1997).
 - ²³ Y. Harashima, K. Terakura, H. Kino, S. Ishibashi, First-Principles Study of Structural and Magnetic Properties of $\text{R}(\text{Fe,Ti})_{12}$ and $\text{R}(\text{Fe,Ti})_{12}\text{N}$ ($\text{R}=\text{Nd, Sm, Y}$), JPS Conf. Proc. **5**, 0111021 (2015).
 - ²⁴ C. Skelland T. Ostler, S. C. Westmoreland, R. F. L. Evans, R. W. Chantrell, M. Yano, T. Shoji, A. Manabe, A. Kato, M. Ito, M. Winklhofer, G. Zimanyi, J. Fischbacher, T. Schrefl, and G. Hrkac, Probability Distribution of Substituted Titanium in RT_{12} ($\text{R} = \text{Nd}$ and Sm ; $\text{T} = \text{Fe}$ and Co) Structures, IEEE Trans. Mag. **54**, 2103405 (2018) and references therein; G. Hrkac, private communications (2019).
 - ²⁵ M. Avdeev and J. R. Hester, ECHIDNA: A decade of high-resolution neutron powder diffraction at OPAL, J. Appl. Cryst. **51**, 1597 (2018).
 - ²⁶ H. M. Rietveld, A Profile Refinement Method for Nuclear and Magnetic Structures, J. Appl. Cryst. **2**, 65 (1969).
 - ²⁷ H. Shiba, A reformulation of the coherent potential approximation and its approximations, Prog. Theor. Phys. **46**, 77 (1971); H. Akai, Residual resistivity of Ni-Fe, Ni-Cr and other ferromagnetic alloys, Physica **86-88B**, 539 (1977).
 - ²⁸ S. H. Vosko, L. Wilk, and M. Nusair, Accurate spin-dependent electron liquid correlation energies for local spin density calculations: a critical analysis, Can. J. Phys. **58**, 1200 (1980).
 - ²⁹ M. Ito (Toyota Motor Corporation), private communications (2018).
 - ³⁰ for a review on the subtlety caused by the temperature dependence of the lattice constants in $4f$ - $3d$ intermetallic ferromagnets, see e.g. A. V. Andreev, Thermal expansion anomalies and spontaneous magnetostriction in rare-earth intermetallics with cobalt and iron, Handbook of Magnetic Materials, Ed. K. H. J. Buschow, Vol. 8, Chap. 2 (1995).
 - ³¹ T. Ishikawa, H. Nagara, K. Kusakabe, and N. Suzuki, Determining the structure of phosphorus in phase IV, Phys. Rev. Lett. **96**, 095502 (2006); H. Fujihisa, Y. Akahama, H. Kawamura, Y. Ohishi, Y. Gotoh, H. Yamawaki, M. Sakashita, S. Takeya, and K. Honda, Incommensurate structure of phosphorus phase IV, Phys. Rev. Lett. **98**, 175501 (2007); T. Ishikawa, private communications (2019).
 - ³² For a recent development combining *ab initio* calculations with experimental data, see N. Tsujimoto, D. Adachi, R. Akashi, S. Todo, S. Tsuneyuki, Crystal structure prediction supported by incomplete experimental data, Phys. Rev. Mater. **2**, 053801 (2018).
 - ³³ M. Matsumoto, H. Akai, Y. Harashima, S. Doi, and T. Miyake, Relevance of $4f$ - $3d$ exchange to finite-temperature magnetism of rare-earth permanent magnets: An *ab-initio*-based spin model approach for NdFe_{12}N , J. Appl. Phys. **119**, 213901 (2016).
 - ³⁴ Y. Harashima, K. Terakura, H. Kino, S. Ishibashi, T. Miyake, First-principles study on stability and magnetism of $\text{NdFe}_{11}M$ and $\text{NdFe}_{11}MN$ for $M = \text{Ti, V, Cr, Mn, Fe, Co, Ni, Cu, Zn}$, J. Appl. Phys. **120**, 203904 (2016).
 - ³⁵ O. Moze, L. Pareti, M. Solzi, W. I. F. David, Neutron diffraction and magnetic anisotropy study of Y-Fe-Ti intermetallic compounds, Solid State Communications **66**, 465 (1988).
 - ³⁶ For a recent review, see e.g. A. W. Sandvik, Stochastic series expansion methods, in E. Pavarini, E. Koch, and S. Zhang (eds.) *Many-Body Methods for Real Materials Modeling and Simulation* Vol. 9, Chap. 16, Forschungszentrum Jülich (2019).
 - ³⁷ J. C. Slater, The ferromagnetism of nickel II. temperature effects, Phys. Rev. **49**, 931 (1936).
 - ³⁸ L. Pauling, The nature of the interatomic forces in metals, Phys. Rev. **54**, 899 (1938).
 - ³⁹ R. M. Bozorth, *Ferromagnetism* (Wiley-IEEE Press, 1993).
 - ⁴⁰ N. F. Mott, Electrons in transition metals, Adv. Phys. **13**, 325 (1964).
 - ⁴¹ J. B. Staunton, The electronic structure of magnetic transition metallic materials, Rep. Prog. Phys. **57**, 1289 (1994).
 - ⁴² S. Chikazumi, *Physics of Ferromagnetism* (Oxford University Press, Clarendon, 1997).
 - ⁴³ J. Kübler, *Theory of Itinerant Electron Magnetism* (Oxford University Press, Clarendon, 2000).
 - ⁴⁴ <http://www.openmx-square.org/>
 - ⁴⁵ T. Ozaki, Variationally optimized atomic orbitals for large-scale electronic structures, Phys. Rev. B. **67**, 155108, (2003).
 - ⁴⁶ T. Ozaki and H. Kino, Numerical atomic basis orbitals from H to Kr, Phys. Rev. B **69**, 195113 (2004).
 - ⁴⁷ T. Ozaki and H. Kino, Efficient projector expansion for the *ab initio* LCAO method, Phys. Rev. B **72**, 045121 (2005).
 - ⁴⁸ T. V. T. Duy and T. Ozaki, A three-dimensional domain decomposition method for large-scale DFT electronic structure calculations, Comput. Phys. Commun. **185**, 777

- (2014).
- ⁴⁹ K. Lejaeghere, G. Bihlmayer, T. Björkman, P. Blaha, S. Blügel, V. Blum, D. Caliste, I.E. Castelli, S.J. Clark, A. Dal Corso, S. de Gironcoli, T. Deutsch, J.K. Dewhurst, I. Di Marco, C. Draxl, M. Dulak, O. Eriksson, J.A. Flores-Livas, K.F. Garrity, L. Genovese, P. Giannozzi, M. Giantomassi, S. Goedecker, X. Gonze, O. Grånäs, E.K. Gross, A. Gulans, F. Gygi, D.R. Hamann, P.J. Hasnip, N.A. Holzwarth, D. Iusan, D.B. Jochym, F. Jollet, D. Jones, G. Kresse, K. Koepernik, E. Küçükbenli, Y.O. Kvashnin, I.L. Locht, S. Lubeck, M. Marsman, N. Marzari, U. Nitzsche, L. Nordström, T. Ozaki, L. Paulatto, C.J. Pickard, W. Poelmans, M.I. Probert, K. Refson, M. Richter, G.M. Rignanese, S. Saha, M. Scheffler, M. Schlipf, K. Schwarz, S. Sharma, F. Tavazza, P. Thunström, A. Tkatchenko, M. Torrent, D. Vanderbilt, M.J. van Setten, V. Van Speybroeck, J.M. Wills, J.R. Yates, G.X. Zhang, and S. Cottenier, Reproducibility in density functional theory calculations of solids, *Science* **351**, aad3000 (2016).
 - ⁵⁰ I. Morrison, D. M. Bylander, L. Kleinman, Nonlocal Hermitian norm-conserving Vanderbilt pseudopotential, *Phys. Rev. B* **47**, 6728 (1993).
 - ⁵¹ G. Theurich and N.A. Hill, Self-consistent treatment of spin-orbit coupling in solids using relativistic fully separable *ab initio* pseudopotentials, *Phys. Rev. B* **64**, 073106 (2001).
 - ⁵² M. Matsumoto, Site preference of substitute elements in $\text{Nd}_2\text{Fe}_{14}\text{B}$, preprint [arXiv:1812.10945].
 - ⁵³ K. J. Strnat and R. M. W. Strnat, Rare earth-cobalt permanent magnets, *J. Magn. Magn. Mater.* **100**, 38 (1991).
 - ⁵⁴ H. Fujii and H. Sun, Interstitially modified intermetallics of rare earth and 3d elements, *Handbook of Magnetic Materials*, Ed. K. H. J. Buschow, Vol. 9, Chap. 3 (1995).
 - ⁵⁵ H. S. Li and J. M. D. Coey, Magnetic properties of ternary rare-earth transition-metal compounds, *Handbook of Magnetic Materials*, Ed. K. H. J. Buschow, Vol. 6, Chap. 1 (1991).
 - ⁵⁶ J. Korringa, On the calculation of the energy of a Bloch wave in a metal, *Physica* **13**, 392 (1947); W. Kohn and N. Rostoker, Solution of the Schrödinger equation in periodic lattices with an application to metallic lithium, *Phys. Rev.* **94**, 1111 (1954).
 - ⁵⁷ <http://kkr.iissp.u-tokyo.ac.jp>
 - ⁵⁸ J. Rodríguez-Carvajal, Recent advances in magnetic structure determination by neutron powder diffraction, *Physica B* **192**, 55 (1993).
 - ⁵⁹ L. Bessais and C. Djega-Mariadassou, Structure and magnetic properties of nanocrystalline $\text{Sm}(\text{Fe}_{1-x}\text{Co}_x)_{11}\text{Ti}$ ($x \leq 2$), *Phys. Rev. B* **63**, 054412 (2001).
 - ⁶⁰ A. J. Pindor, J. Staunton, G. M. Stocks, and H. Winter, Disordered local moment state of magnetic transition metals: a self-consistent KKR CPA calculation, *J. Phys. F: Met. Phys.* **13**, 979 (1983).
 - ⁶¹ B. L. Gyorffy, A. J. Pindor, J. Staunton, G. M. Stocks, and H. Winter, A first-principles theory of ferromagnetic phase transitions in metals, *J. Phys. F: Met. Phys.* **15**, 1337 (1985).
 - ⁶² J. Staunton, B. L. Gyorffy, A. J. Pindor, G. M. Stocks, and H. Winter, Electronic structure of metallic ferromagnets above the Curie temperature, *J. Phys. F: Met. Phys.* **15**, 1387 (1985).
 - ⁶³ J. Staunton, B. L. Gyorffy, G. M. Stocks, and J. Wadsworth, The static, paramagnetic, spin susceptibility of metals at finite temperatures, *J. Phys. F: Met. Phys.* **16**, 1761 (1986).
 - ⁶⁴ J. B. Staunton, S. Ostanin, S. S. A. Razee, B. L. Gyorffy, L. Szunyogh, B. Ginatempo, and Ezio Bruno, Temperature dependent magnetic anisotropy in metallic magnets from an *ab initio* electronic structure theory: L_{10} -ordered FePt, *Phys. Rev. Lett.* **93**, 257204 (2004).
 - ⁶⁵ J. B. Staunton, L. Szunyogh, Á. Buruzs, B. L. Gyorffy, S. Ostanin, and L. Udvardi, Temperature dependence of magnetic anisotropy: An *ab initio* approach, *Phys. Rev. B* **74**, 144411 (2006).
 - ⁶⁶ C. E. Patrick, J. B. Staunton, Temperature-dependent magnetocrystalline anisotropy of rare earth/transition metal permanent magnets from first principles: The light $R\text{Co}_5$ ($R=\text{Y, La-Gd}$) intermetallics, *Phys. Rev. Mater.* **3**, 101401(R) (2019).
 - ⁶⁷ T. Hawai *et al.*, in preparation.
 - ⁶⁸ Y. Tokura, H. Takagi, S. Uchida, A superconducting copper oxide compound with electrons as the charge carriers, *Nature* **337**, 345 (1989).
 - ⁶⁹ for a recent review, see M. Naito, Y. Krockenberger, A. Ikeda, H. Yamamoto, Reassessment of the electronic state, magnetism, and superconductivity in high-Tc cuprates with the Nd_2CuO_4 structure, *Physica C* **523**, 28 (2016).
 - ⁷⁰ for a review, see P. A. Lee, N. Nagaosa, and X.-G. Wen, Doping a Mott insulator: Physics of high-temperature superconductivity, *Rev. Mod. Phys.* **78**, 17 (2006).
 - ⁷¹ for a review, see M. Imada, A. Fujimori, Y. Tokura, Metal-insulator transitions, *Rev. Mod. Phys.* **70**, 1039 (1998).